The response of soft tissue cells to Ti implants is modulated by blood-implant interactions

William A. Lackington [a], Lada Fleyshman [a], Peter Schweizer [b], Yvonne Elbs-Glatz [a], Stefanie Guimond [a], Markus Rottmar [a,*]

[a] Biointerfaces Laboratory, Empa, Swiss Federal Laboratories for Materials Science and Technology, St. Gallen, Switzerland
[b] Mechanics of Materials & Nanostructures Lab, Empa, Swiss Federal Laboratories for Materials Science and Technology, Thun, Switzerland

ABSTRACT

Titanium-based dental implants have been highly optimized to enhance osseointegration, but little attention has been given to the soft tissue-implant interface, despite being a major contributor to long term implant stability. This is strongly linked to a lack of model systems that enable the reliable evaluation of soft tissue-implant interactions. Current *in vitro* platforms to assess these interactions are very simplistic, thus suffering from limited biological relevance and sensitivity to varying implant surface properties. The aim of this study was to investigate how blood-implant interactions affect downstream responses of different soft tissue cells to implants *in vitro*, thus taking into account not only the early events of blood coagulation upon implantation, but also the multicellular nature of soft tissue. For this, three surfaces (smooth and hydrophobic; rough and hydrophobic; rough and hydrophilic with nanostructures), which reflect a wide range of implant surface properties, were used to study blood-material interactions as well as cell-material interactions in the presence and absence of blood. Rough surfaces stimulated denser fibrin network formation compared to smooth surfaces and hydrophilicity accelerated the rate of blood coagulation compared to hydrophobic surfaces. In the absence of blood, smooth surfaces supported enhanced attachment of human gingival fibroblasts and keratinocytes, but limited changes in gene expression and cytokine production were observed between surfaces. In the presence of blood, rough surfaces supported enhanced fibroblast attachment and stimulated a stronger anti-inflammatory response from macrophage-like cells than smooth surfaces, but only smooth surfaces were capable of supporting long-term keratinocyte attachment and formation of a layer of epithelial cells. These findings indicate that surface properties not only govern blood-implant interactions, but that this can in turn also significantly modulate subsequent soft tissue cell-implant interactions.

1. Introduction

Dental implants are routinely used in modern oral maxillofacial surgery, with more than 5 million individual implants being placed in the US annually and a growing market estimated to be worth over USD 10 billion [1]. Ideally, dental implants should achieve long-term mechanical stability, which is determined by how they integrate with both soft tissue and underlying supporting bone [2,3]. Titanium (Ti) and its alloys have been widely used for dental implants due to their cytocompatibility and their tough mechanical properties [4]. Ti surface properties have been highly optimized to support osseointegration [5,6], to ultimately enhance the clinical success rate of implants [7]. However, despite being a key factor for long term implant stability, less attention has been given

to the interface between implants and soft tissue [2,8]. Peri-implantitis, the destructive inflammation of the soft tissue-implant interface, is one of the main driving factors of implant failure [9,10]. With this in mind, investigating how dental implant surface properties impact the response of soft tissue cells is highly warranted, as it could inform the development of future implants to mitigate the effects of peri-implantitis.

In vitro platforms to study osseointegration have facilitated advances in the development of implant surfaces for dental applications [11–13]. To this end, increasing hydrophilicity and higher surface roughness have been demonstrated to enhance osteoblast proliferation and improve the osseointegration potential, in comparison to hydrophobic and smoother surfaces [14–16]. However, when assessing soft tissue-implant interactions, even sophisticated 3D *in vitro* platforms suffer from limited

biological relevance and sensitivity to varying implant surface properties [17]. Some more simplified studies in 2D have shown that surface roughness is an important parameter for the attachment and growth of gingival fibroblasts [18,19] and keratinocytes [20], suggesting that smoother or finely grooved Ti surfaces are favourable for soft tissue integration compared to rougher surfaces [21,22]. Conversely, rougher surfaces were shown to stimulate macrophage activation towards an anti-inflammatory (M2-like) phenotype, while smoother surfaces promote a pro-inflammatory (M1-like) phenotype [15,23]. Collectively, previous studies highlight that there is a lack of consensus on the ideal surface properties to stimulate healthy soft tissue integration. Additionally, these studies in 2D share the common limitation that their implications for soft tissue-implant integration are based on findings from a single cell type and that blood-implant interactions are not taken into account.

When placing an implant, blood emerges from the wound and comes into contact with the implant, resulting in protein adsorption and eventually blood coagulation. Thus, cells from the surrounding tissue never see the bare implant material. Despite this, blood-implant interactions are generally omitted from *in vitro* studies, thus potentially reducing the biological relevance of their findings. In the context of osseointegration, pre-incubation of implant surfaces with human whole blood, prior to seeding bone progenitor cells, has demonstrated the capacity to improve the biological relevance of *in vitro* findings, while yielding a high degree of correlation with *in vivo* data [11,16,24]. Specifically, the adsorption of blood plasma proteins, platelet adhesion and activation, as well as the release of wound healing growth factors and the formation of a blood fibrin network on an implant surface, is correlated with improved mineralization [11,16]. Thus, while blood-implant interactions might be of biological relevance for the subsequent response of soft tissue cells, as has been suggested in a study investigating the interaction between dermal fibroblasts and blood clot formation [25], their impact on gingival fibroblasts, keratinocytes, and macrophages currently remains poorly understood.

The central hypothesis of this study is that blood-implant interactions have a major influence on the quality of the soft tissue-implant interface, resulting in increased biological sensitivity of gingival cells to changes in surface properties. Ti implant surfaces that are both clinically available and have a wide range of surface properties were used to study the biological response of human gingival fibroblasts (HGFs), gingival keratinocytes (HGKs), and THP-1-derived macrophage-like cells, with and without a pre-incubation step in human whole blood. The surfaces used include Machined (smooth and hydrophobic), SLA-H$_{phob}$ (rough and hydrophobic), and SLActive-H$_{phil}$NS (rough, hydrophilic, and with nanostructures). Blood-implant interactions were assessed in terms of fibrin network formation and cytokine production (IL-8, IL-6, VEGF and TNF-α). Cell-implant interactions, in the presence and absence of blood, were evaluated in terms of cell attachment, morphology and size, metabolic activity and total DNA content, cytokine production, and gene expression of pro- and anti-inflammatory markers (*CXCL10* and *CD206*). This approach facilitated decoupling of the effects of Ti implant surface properties on blood-implant and cell-implant interactions, providing a more biologically relevant *in vitro* platform for the evaluation of soft tissue integration.

2. Materials and methods

2.1. Cell culture

Primary human gingival fibroblasts (HGFs, ScienCell, USA) were expanded in growth medium consisting of Dulbecco's Modified Eagle's Medium (DMEM, 4.5 g/L glucose, Sigma, Switzerland) with 10% foetal bovine serum (FBS, Sigma) and 1% penicillin – streptomycin (P/S, 5 mg/mL, Sigma).

Primary human gingival epithelial cells (HGEPps, CELLnTEC, Switzerland) representing human gingival keratinocytes (HGKs) were expanded in keratinocyte medium (CnT-57; CELLnTEC).

A human monocytic leukaemia cell line (THP-1, ECACC 88081201, UK) was used to generate macrophage-like cells. THP-1 cells were expanded in growth medium consisting of RPMI 1640 Medium (Sigma) supplemented with 10% FBS, 1% P/S and 1% L-glut (360 mg/mL, Sigma), and differentiated into macrophage-like cells by supplementing the medium with 100 nM phorbol myristate acetate (PMA; Sigma) for 3 days. To stimulate a pro-inflammatory (M1-like) phenotype, macrophages were subjected to 100 ng/mL LPS (Sigma) and 20 ng/mL interferon-γ (Miltenyi Biotec, Switzerland), while to stimulate an anti-inflammatory (M2-like) phenotype, 20 ng/mL interleukin-4 (Miltenyi Biotec) was used, as previously reported [26].

HGFs, HGKs, and THP-1 cells were cultured at 37 °C with 5% of CO$_2$. Growth medium was changed every three days and cells were passaged at 70–90% confluency. Subculture passages 1 to 8 were used for experiments involving HGFs and HGKs, while THP-1 cells were used between passage 6 and 18.

2.2. Ti surface pre-incubation with human whole blood

Three types of titanium grade 4 discs (5 mm diameter and 1 mm height) with clinically used dental implant surface modifications were used in this study: Machined, SLA-H$_{phob}$ and SLActive-H$_{phil}$NS, kindly provided by Institut Straumann AG (Switzerland). Machined samples are produced via a grinding process, SLA is a commercially available sandblasted, large-grit, acid etched surface, while SLActive is chemically modified SLA that exhibits increased hydrophilicity and features nanostructures [27,28]. The contact angle was evaluated by contact-angle measurements using a sessile-drop test with ultrapure water (EasyDrop DSA20E, Krüss GmbH) and a droplet size of up to 0.3 μL. The roughness was analyzed using a confocal microscope (μsurf explorer, NanoFocus AG), with a measurement area of 798 × 798 μm^2 and a lateral resolution of 1.56 μm. Roughness values were determined by applying a Gaussian filter with a cut-off wavelength of 50 μm. All discs were sterilized using gamma sterilization.

Ti surfaces were pre-incubated with partially heparinized (0.5 IU/mL, Sigma) human whole blood, taken from healthy male and female donors aged 18–55 years (ethical approval was obtained from the local ethics committee; EKSG, BASEC Nr PB_2016_00816) and used within 1 h after withdrawal. Each experiment was repeated at least 3 times with different donors each time. The time for blood clot formation was estimated individually for each donor using SLActive-H$_{phil}$NS as a reference as described previously [24] and was found to be generally between 15 and 30 min. Samples were incubated with blood in custom-made Teflon moulds, washed with phosphate buffered saline (PBS, Sigma) three times and transferred to a 96-well plate format for seeding of HGFs, HGKs, or macrophage-like cells. HGFs and HGKs were seeded at a density of 20,000 cells/cm^2, while macrophage-like cells were seeded at a density of 250,000 cells/cm^2 in basal medium without M1 or M2 stimulation factors. For comparison, macrophage-like cells were also seeded on TCP, where they were stimulated with M1 and M2 factors for 24 h. After 24 h, cell seeded Ti samples were transferred to new wells for the remaining culture period.

2.3. Analysis of blood- and cell-implant interactions

Scanning electron microscopy (SEM) was used to assess the topography of the Ti implant surfaces, fibrin network formation, and cell attachment on different surfaces. Ti samples were fixed with Karnovsky solution (4% paraformaldehyde, 2.5% glutaraldehyde) for 1 h and washed twice with PBS after 1 day in culture. Samples were dehydrated in an increasing gradient of ethanol (EtOH) as follows: 50%, 70%, and 80% EtOH for 30 min, 90% and 100% EtOH for 60 min, and finally in hexamethyldisilazane (Sigma) for 30 min, and left to dry overnight. Samples were sputter coated with a 5 nm layer of gold/palladium (EM ACE600, Leica Microsystems, Switzerland) before imaging at an

accelerating voltage of 2.0 kV (Hitachi S-4800, Hitachi-High Technologies).

Confocal laser scanning microscopy (CLSM) was also used to assess fibrin network formation and cell attachment on Ti implant surfaces. After 1, 3 and 7 days post-seeding, samples were fixed with 4% paraformaldehyde (4% PFA; 25 mM HEPES, 10 mM EDTA, 3 mM MgCl$_2$, 65 mM PIPES) for 30 min and then permeabilized with 0.1% Triton X (Sigma) for 30 min. Samples were stained with mouse anti-fibrinogen (1:200, ThermoFisher), or mouse anti-vinculin (1:200, ThermoFisher), followed by anti-mouse Alexa Fluor 555 (1:200, ThermoFisher) antibodies. Cell nuclei and actin filaments were then counter stained with 4′,6-diamidino-2-phenylindole (1:500, DAPI, Sigma), and Alexa Fluor 488-conjugated phalloidin (1:200, ThermoFisher). Samples were imaged on a LSM 780 (Zeiss, Germany) and the average cell size was obtained using ImageJ, as previously described [29].

TEM cross-sections were prepared using a Tescan Lyra focused ion beam system. TEM images were acquired at 200 keV with a Thermo Scientific Titan Themis 200 G3. EDX was used to differentiate between the various organic components (erythrocytes, fibrin network, and HGFs) on the Ti implant surface, and the images were manually segmented using this information.

2.4. Assessment of cell proliferation on Ti surfaces

Cell proliferation of HGFs, HGKs, and macrophage-like cells, was evaluated in this study using a metabolic activity assay (PrestoBlue assay, ThermoFisher) and dsDNA quantification (PicoGreen assay, Thermo-Fisher) following the manufacturer's instructions. In brief, after transferring samples to a new 96-well plate at each timepoint, metabolic activity of cells on Ti surfaces was determined using the PrestoBlue reagent at days 1, 3, and 7 post-seeding. Fluorescence was measured with excitation and emission wavelengths set at 560 and 590 nm (Mithras2 plate reader, Berthold Technologies). The dsDNA mass of cells on Ti surfaces was determined at days 1 and 7 post-seeding for HGFs and HGKs, and at days 1 and 3 post-seeding for macrophage-like cells (due to their short activity). The dsDNA levels from blood cells on samples was determined and subtracted from the levels recorded from samples cultured with both blood and cells. The reported metabolic activity levels come with the caveat that they include both the metabolic activity of blood cells and the cells subsequently seeded on the surface.

2.5. Evaluation of cytokine production by cells on Ti surfaces

The production of inflammatory and wound healing-related cytokines by HGFs, HGKs, and macrophage-like cells, was evaluated using the culture medium collected from samples after 3 and 7 days (1 and 3 days for macrophage-like cells). Cytokine concentrations of interleukin-8 (IL-8), interleukin-6 (IL-6), tumour necrosis factor-alpha (TNF-α), and vascular endothelial growth factor (VEGF), were quantified using enzyme-linked immunosorbent assays (ELISA) (Invitrogen, Switzerland), following the manufacturer's protocol. The cytokine levels produced by blood cells on samples were determined and subtracted from the levels recorded from samples cultured with both blood and cells.

2.6. Evaluation of macrophage-like cell gene expression on Ti surfaces

After 24 h of culture, macrophage-like cells on Ti discs were lysed and RNA was isolated using the RNeasy Mini Kit (Qiagen, Germany), according to the manufacturer's protocol. The RNA from 3 replicate samples was pooled before assessing RNA concentration and quality using a Nanodrop ND-1000 Spectrometer (Thermo Scientific). RNA (400 ng) was transcribed to cDNA using the iScript cDNA synthesis kit (Bio-Rad, Switzerland). A temperature profile of 5 min priming at 25 °C, followed by reverse transcription at 42 °C for 30 min, and inactivation at 85 °C for 5 min was performed. After cooling down to 4 °C, the cDNA was diluted in RNAse free water to a final concentration of 1.5 ng/μL and stored at −80 °C for subsequent use.

Based on our previously reported investigation of M1 and M2 markers using the same macrophage-like cells [26], real time-qPCR reactions were set up to evaluate the gene expression of anti-inflammatory M2 markers PPAR-γ, CD206, CCL22, and IL-10, as well as pro-inflammatory M1 markers TNF-α and CXCL10. Reactions were performed according to the manufacturer's protocol using the iQ SYBR Green Supermix kit (Bio-Rad), with the primers listed in the Table below (Table 1). Reactions were carried out with the CFX Opus 384 RT-PCR System (Bio-Rad). Each reaction was made up to a total volume of 12 μL, consisting of 5 μL cDNA, 0.24 μL forward and reverse primers (10 μM), 6 μL mastermix, and 0.52 μL RNAnase-free water. The reaction consisted of denaturation at 95 °C for 5 min, annealing at 60 °C for 30 s, and ran for 40 cycles. The expression of target genes was normalized to the expression of housekeeping gene GAPDH. Relative gene expression was determined using the $2^{-\Delta\Delta Ct}$ method, and the second delta was calculated relative to gene expression of cells on the Machined surface in the absence of blood.

2.7. Statistical analyses

Results are expressed as mean ± standard deviation, unless otherwise stated. Analysis of the statistical significance between groups was performed by one-way ANOVA (for a single timepoint) or two-way ANOVA (for two or more timepoints). Results were obtained from experiments that were repeated at least 3 times, with different blood donors each time. All statistical analyses were performed using GraphPad Prism 8 (GraphPad Software Inc., USA). To determine the average cell size, the data from 250 to 1200 cells was used. Asterisks denote statistical significance as follows: *p < 0.05, **p < 0.01, ***p < 0.001, and p < 0.0001.

3. Results and discussion

3.1. Implant surface properties can steer blood-implant interactions

Blood is the first tissue an implant surface will interact with upon implantation, and this interaction has been shown to significantly alter the response of bone progenitor cells to implants [11,24]. Therefore, taking blood-implant interactions into account could potentially improve the physiological relevance of *in vitro* findings also in the context of soft tissue integration [30]. Conversely, blood-implant interactions are highly dependent on surface properties, including wettability and roughness.

Table 1
List of primers used for qPCR analysis.

Target gene	Forward Primer (5′-3′)	Reverse Primer (5′-3′)
GAPDH	AGTCAGCCGCATCTTCTTTT	CCAATACGACCAAATCCGTTG
PPARγ	TTGCTGTCATTATTCTCAGTGGAG	GAGGACTCAGGGTGGTTCAGC
CD206	GCTACCCCTGCTCCTGGTTT	CGCAGCGCTTGTGATCTTCA
TNFα	CCGTCTCCTACCAGACCAAG	CTGAGTCGGTCACCCTTCTC
CXCL10	CAGTCTCAGCACCATGAATCAA	CAGTTCTAGAGAGAGGTACTCCTTG
CCL22	GCGTGGTGTTGCTAACCTTC	CCACGGTCATCAGAGTAGGC
IL-10	ACATCAAGGCGCATGTGAAC	CAGGGAAGAAATCGATGACAGC

Table 2
Summary of Ti implant surface properties used in this study.

	Machined	SLA-H_{phob}	SLActive-H_{phil}NS
Contact angle (°)	93.6 ± 3	126.7 ± 2	0
Roughness, R_a (µm)	0.07 ± 0.01	1.56 ± 0.09	1.43 ± 0.41

The surface contact angle and roughness for each implant surface are listed in Table 2. SLA-H_{phob} and SLActive-H_{phil}NS had similar rougher surfaces compared to Machined, while Machined and SLA-H_{phob} were hydrophobic in comparison to hydrophilic SLActive-H_{phil}NS. Taken together, this group of implant surfaces provided a suitable wide range of surface properties to further proceed with the study.

Surface topography has been shown to have an influence on protein adsorption, with some studies suggesting that rougher surfaces promote greater protein adsorption compared smoother ones [31]. Analysing the topographies of implant surfaces (Fig. 1A), the Machined surface was relatively smooth in comparison to the rougher SLA-H_{phob} and SLActive-H_{phil}NS surfaces, and presented aligned, longitudinal, microscale features. These surface features appeared shallow and homogenously distributed throughout the surface. The SLA-H_{phob} surface presented a rougher topography than the Machined surface, with a high density of protruding microscale features, which were heterogeneously distributed. The SLActive-H_{phil}NS surface showed similar microscale features as the SLA-H_{phob} surface, but at higher magnification (40kX), the presence of nanoscale features could be observed on SLActive-H_{phil}NS. These nanoscale features, in combination with surface hydrophilicity, were expected to stimulate greater adsorption of fibrinogen to the implant [32].

Upon incubation in human whole blood, the rate of fibrin network formation was found to be dependent on the surface properties of the Ti implant (Fig. 1B and C). Using a time series, the dynamics of the blood response could be revealed. Comparatively, the SLActive-H_{phil}NS surface led to the fastest generation of a dense and homogenously distributed fibrin network, while on the Machined surface only a limited and heterogeneously distributed fibrin network could be seen even at the longest incubation timepoint. The SLA-H_{phob} surface showed intermediate fibrin network formation. While previous studies generally only compared the response of blood at a single timepoint, the findings are in-line with these reports, which have shown that rougher surfaces with the presence of multiscale micro- and nano-roughness, such as SLActive-H_{phil}NS, can stimulate the formation of denser fibrin networks, compared to smoother surfaces, such as Machined [11,33].

In addition to regulating protein adsorption and fibrin network formation, implant surface properties can also influence the production of immunomodulatory cytokines [34]. Assessing cytokine levels of blood-incubated implant surfaces, vascular endothelial growth factor (VEGF) and tumour necrosis factor alpha (TNFα) were not detected, but interleukin-8 (IL-8) and interleukin-6 (IL-6) showed distinct differences dependent on Ti implant surface properties. IL-8 and IL-6 are well established markers of inflammation [35]. Comparable levels of IL-8 were produced by blood in response to Machined and SLActive-H_{phil}NS, which were higher than the levels produced in response to SLA-H_{phob}. All surfaces supported a constant rate of IL-8 production across 7 days (Fig. 1D). Although not statistically significant, the Machined surface led to enhanced production of IL-6 compared to the SLA-H_{phob} and SLActive-H_{phil}NS surfaces (Fig. 1E). Additionally, IL-6 was
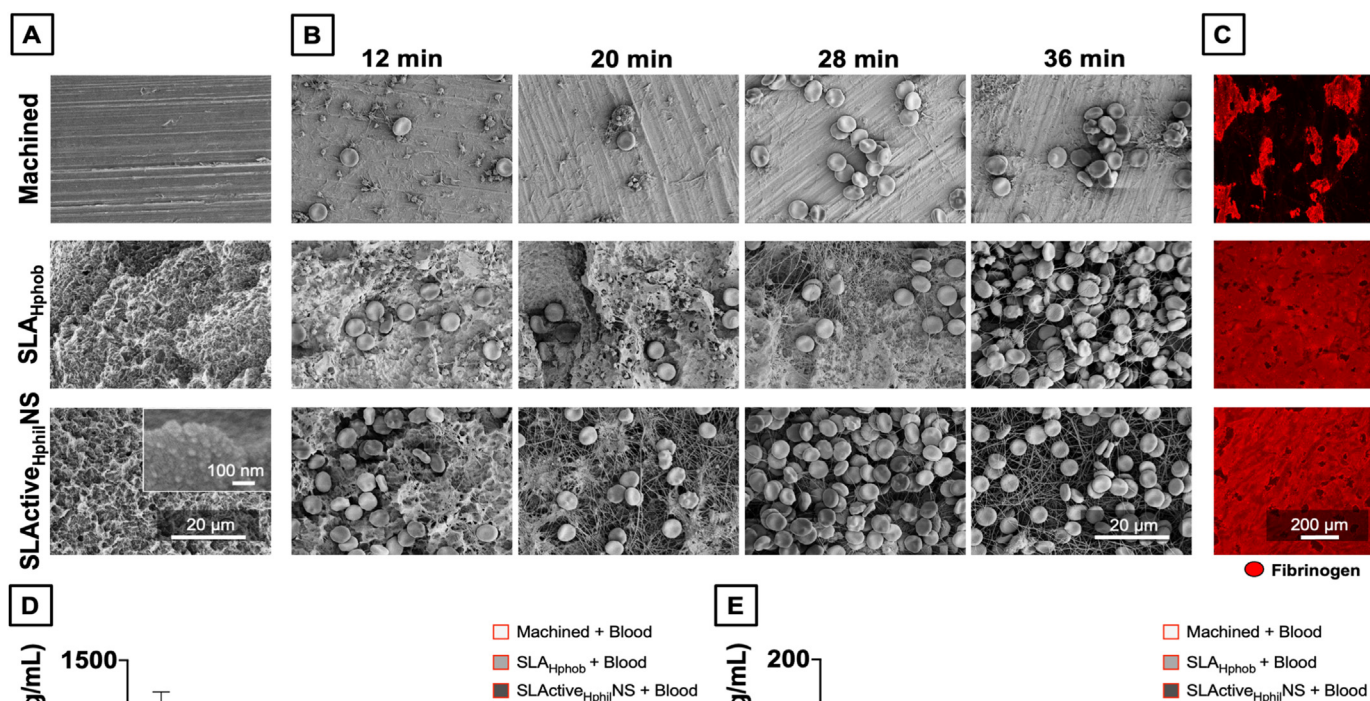

Fig. 1. The effect of Ti implant surface properties on blood-implant interactions. SEM images showing (A) the topography of Machined, SLA-H_{phob}, and SLActive-H_{phil}NS implant surfaces (with an inset showing the presence of nanostructures on the latter) and (B) fibrin network formation on the Ti implant surfaces after incubation with human whole blood for 12, 20, 28 and 36 min. (C) Fibrin network across a 0.67 mm^2 area of the Ti implant surfaces stained for fibrinogen (red), after blood incubation for 28 min. (D) Interleukin-8 production and (E) Interleukin-6 production in response to the Ti implant surfaces, after 1, 3 and 7 days.

found to be produced at higher levels initially, with levels tapering off by day 7.

These results suggest that the production of inflammatory cytokines, IL-8 and IL-6, by blood is inversely related with the density of the fibrin network. The Machined surface, which stimulates the formation of the least dense fibrin network, triggered the highest production of IL-8 and IL-6, which were likely produced by blood monocytes or other peripheral blood mononuclear cells. These findings correlate with those of a recent study, which using isolated peripheral blood mononuclear cells, showed that the Machined surface stimulated a higher production of both IL-8 and IL-6 in comparison to the SLActive-H$_{phil}$NS surface [36]. The current study adds to this by also highlighting that the activity of IL-8 and IL-6 production by blood in response to the Ti surfaces is cytokine-specific, with IL-8 showing a persistent production, whereas IL-6 shows a transient production, which could be due to IL-6's potent self-restricting negative feedback loop mediated by STAT3 in leukocytes [37,38]. Taken together, these findings highlight that

surface-property-dependent blood-implant interactions lead to variable degrees of fibrin network formation, which not only acts as a protein-based support structure, but also as a cytokine reservoir, which then can influence the response of surrounding tissue cells. Additionally, blood-implant interactions could have the potential to influence the susceptibility of an implant towards bacterial infection. Bacterial infection can be mitigated by promoting a strong gingival tissue seal around an implant, but first implants are susceptible towards infection particularly during implantation and soon thereafter. Some studies have investigated the 'race-for-the-surface' between gingival fibroblasts and bacteria for adhesion on designer implant surfaces [18,39,40], highlighting how specific surface properties and topographical features can promote fibroblast cell adhesion while inhibiting bacterial adhesion. This study does not focus on bacteria-implant interactions, but it suggests that the race-for-the-surface can be further steered to prevent bacterial adhesion through blood-implant interactions, including the release of antibacterial peptides or the upregulation of inflammatory cytokines,
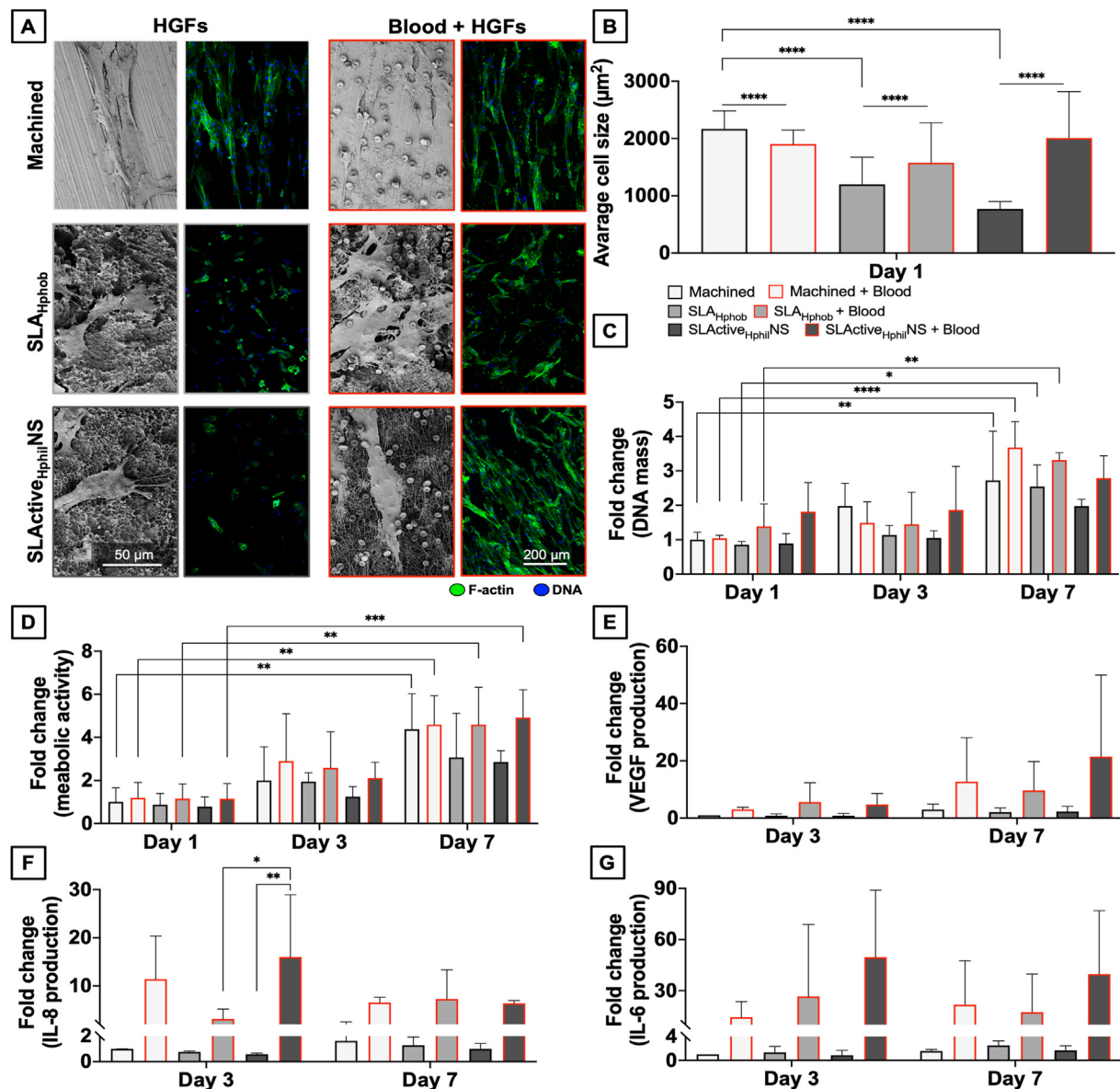
Fig. 2. The effect of blood-implant interactions on the attachment, proliferation, and cytokine production of HGFs in response to Ti implant surfaces. (A) SEM and CLSM images showing the morphology of HGFs attached to the Ti implant surfaces, in the presence and absence of blood, after 24 h. Cells were stained for their cytoskeleton (green) and nuclei (blue). (B) Average cell size of HGFs, in the presence and absence of blood, after 24 h. Fold change of (C) DNA mass and (D) metabolic activity after 1,3 and 7 days, (E) VEGF production, (F) IL-8 production, and (G) IL-6 production after 3 and 7 days normalized to the amount produced by HGFs on the Machined surface.

which can promote the influx of monocytes and other immune cells associated with acute inflammation.

3.2. Blood-implant interactions modulate the response of human gingival fibroblasts to Ti implant surfaces

A number of studies have previously assessed the response of human gingival fibroblasts [18,19], keratinocytes [20], and macrophages [15, 23] to Ti implant surfaces, however none have done so with all 3 cell types under identical conditions in parallel, while only few reports take blood-implant interactions into account [25]. This is addressed herein.

In the absence of blood, the Machined surface promoted enhanced HGF attachment with cells displaying an elongated cell morphology, aligned to the underlying microscale topological features, whereas HGFs on the rougher surfaces (SLA-Hphob and SLActive-H$_{phil}$NS) showed a less dense and stochastic attachment pattern with limited cell spreading. This cell alignment can be explained by the anisotropic deposition of serum proteins on the machined surface [41]. Cell attachment and spreading on the rougher surfaces was enhanced when the implant surface was pre-incubated with blood, whilst on the Machined surface, cell

attachment was similar in both the presence and absence of blood (Fig. 2A). Blood also significantly enhanced the average cell size of HGFs on both of the rough Ti implant surfaces, with a 1.3-fold and 2.6-fold increase in size of HGFs on the SLA-Hphob and the SLActive-H$_{phil}$NS surface, respectively (Fig. 2B). The attachment of HGFs was also enhanced by blood-implant interactions, particularly in the case of rougher surfaces, which stimulated a significant increase in cell size. Previous studies have suggested that there is no significant difference in HGF attachment to rough and smooth Ti implant surfaces after 48 h of culture [18], while others have shown limited attachment of mouse fibroblast cells on rough surfaces [42,43]. In comparison, this study shows significant differences in cell attachment to smooth and rough implant surfaces after only 24 h with smooth implant surfaces supporting enhanced focal adhesion formation (Fig. 3A), and greater cell-to-implant surface contact (Fig. 3B), in comparison to rougher surfaces. Conversely, HGFs on rough surfaces incubated with blood benefit from additional binding sites provided by a dense fibrin network, facilitating greater cell spreading on the surface (Fig. 3B). A similar cell-implant interaction was previously observed for osteoblasts [11].

Blood-implant interactions also stimulated the proliferation of HGFs
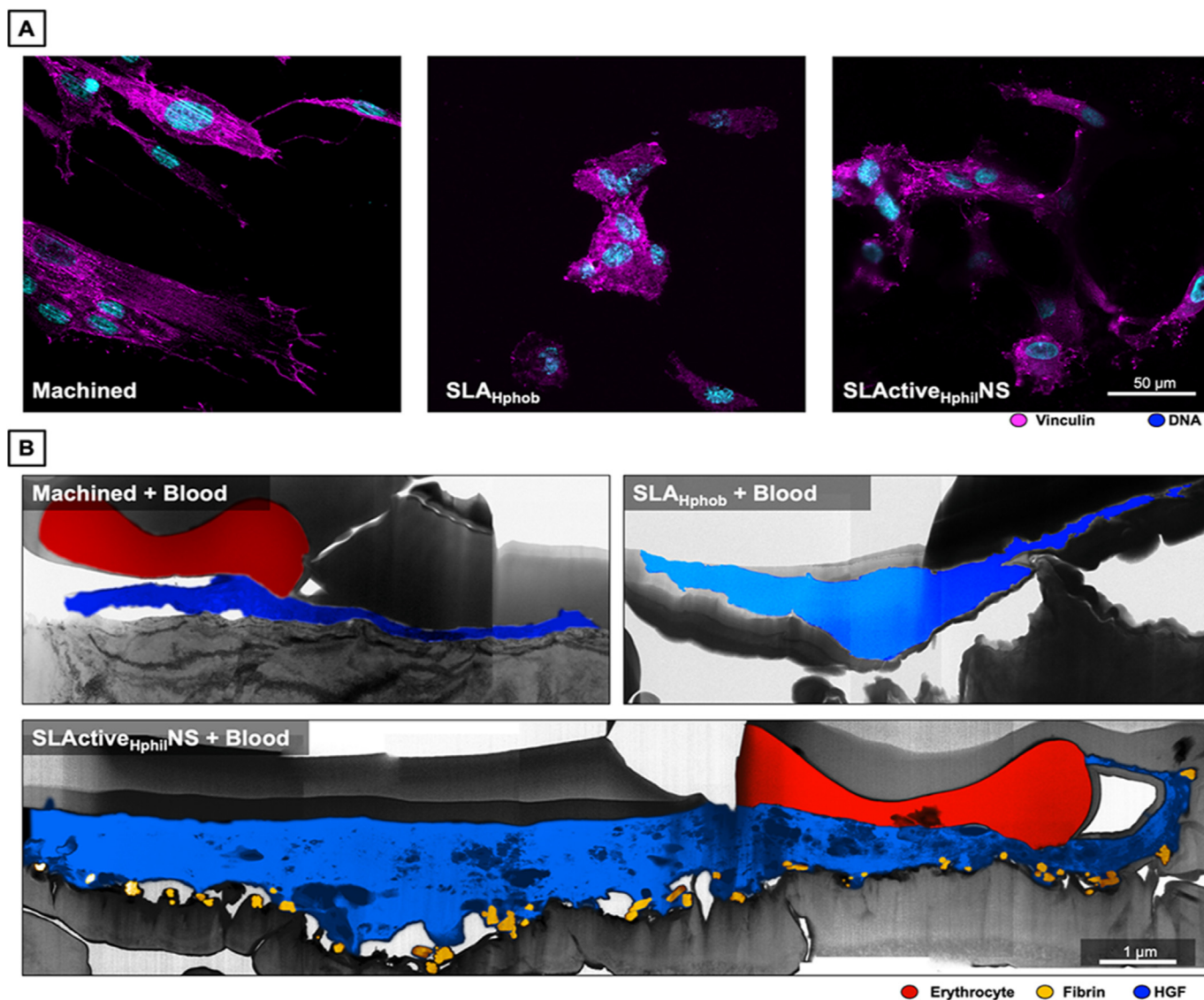
Fig. 3. The attachment of HGFs to Ti implant surfaces in the presence and absence of blood. (A) CLSM images showing focal adhesions formed by HGF in response to the Ti implant surfaces, in the absence of blood, after 24 h. Cells were stained for their focal adhesions (magenta) and nuclei (blue). (B) TEM cross sections depicting the contact points between HGFs and the surface of Ti implants, in the presence of blood, after 24 h.

attached to the Ti implant surfaces (Fig. 2C), in similar ways to the previously reported proliferation of dermal fibroblasts and osteoblasts [11,25]. While all three implant surfaces showed increasing DNA mass of HGFs from day 1–7, significant changes were only observed with the Machined and SLA-H$_{phob}$ surfaces, especially when pre-incubated with blood (Fig. 2C). Similar trends could be observed when measuring the metabolic activity of HGFs (Fig. 2D). The formation of a dense fibrin network and adsorption of blood proteins, including fibrinogen, fibronectin and vitronectin [44,45], can explain the enhanced attachment and proliferation of HGFs to rougher surfaces in the presence of blood, as blood provides an overwhelmingly superior number of attachment sites compared to when the implant surface is cultured in the absence of blood, where only serum can provide proteins for cell attachment.

Assessing cytokine levels of HGFs cultured on the different implant surfaces, in the absence of blood, the Machined surface led to a limited production of vascular endothelial growth factor (VEGF: 80 pg/mL),

interleukin-8 (IL-8: 44 pg/mL), and interleukin-6 (IL-6: 5 pg/mL) after 3 days (Fig. 2E, F, and 2G). In comparison, rougher surfaces did not stimulate an increase of these cytokines by more than 2-fold nor a decrease by less than 0.5-fold. However, blood-implant interactions stimulated the production of VEGF by HGFs to increase by a fold-change of 12.7, 9.7, and 21.5, on the Machined, SLA-Hphob, and SLActive-HphilNS surfaces, respectively, on day 7 (Fig. 2E). Similarly, the production of IL-8 was also enhanced by a fold-change of 11.4, 3.1, and 15.9 (Fig. 2F), and the production of IL-6 by a fold-change of 14.4, 26.6, and 49.6 (Fig. 2G) at day 3. The levels of IL-8 and IL-6 were generally higher at day 3 compared to day 7, where the level of VEGF was highest. The production of TNFα and IL-1β was not stimulated by any surface or condition. Previous studies have shown similar responses in terms of IL-6 production [46] to smooth and rough Ti surfaces; as is the case in this study in the absence of blood. However, this study highlights that in the presence of blood-implant interactions, the response of HGFs to Ti implant surfaces is
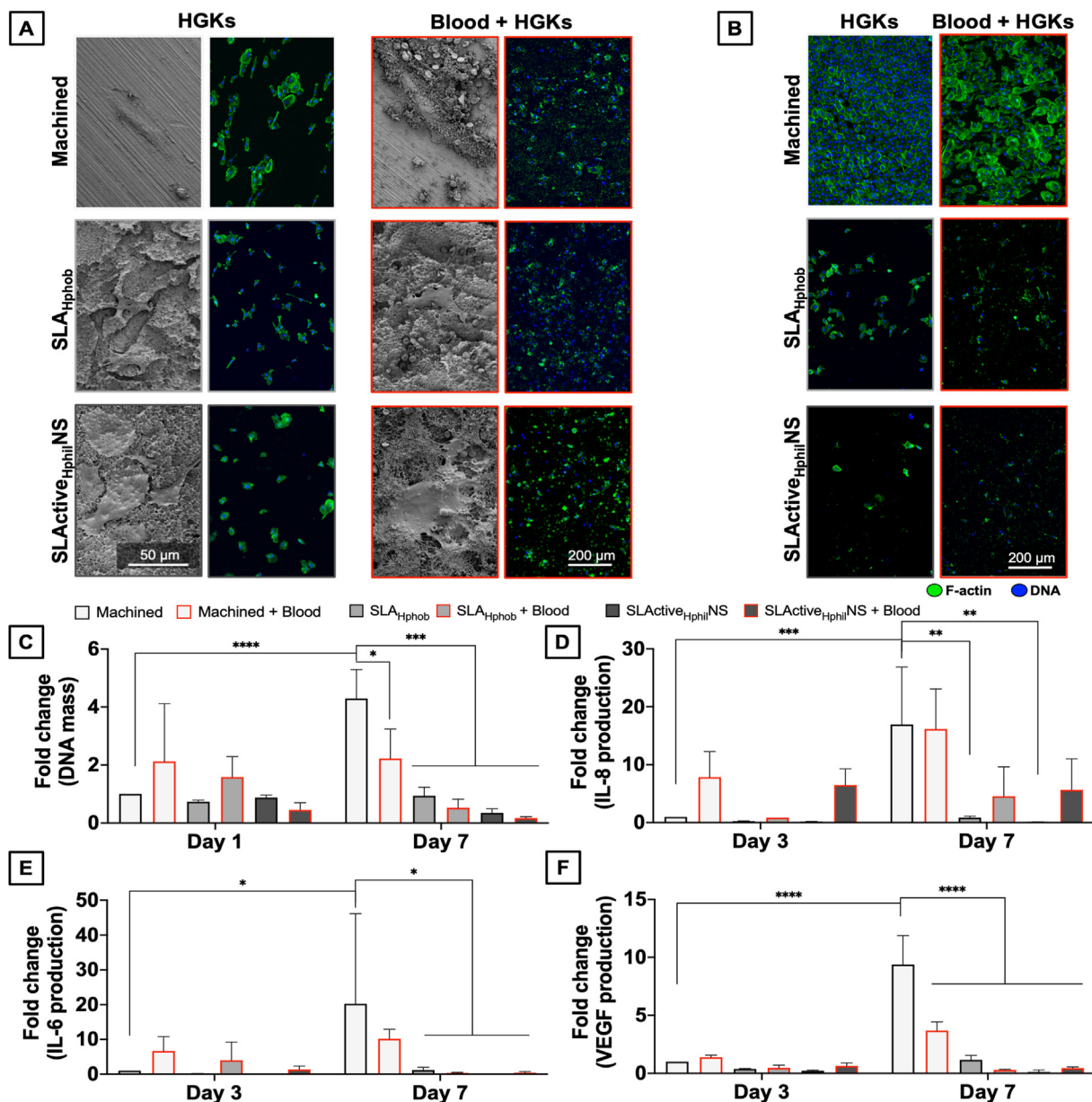

Fig. 4. The effect of blood-implant interactions on the attachment, proliferation, and cytokine production of HGKs in response to Ti implant surfaces. SEM and CLSM images showing the morphology of HGKs, in the presence and absence of blood, after (A) 24 h, and (B) 7 days. Cells were stained for their cytoskeleton (green) and nuclei (blue). Fold change of (C) DNA mass after 1 and 7 days, (D) VEGF production, (E) IL-8 production, and (F) IL-6 production after 3 and 7 days, normalized to the amount produced by HGKs on the Machined surface.

readily modulated, with rougher surfaces stimulating enhanced IL-6 (and IL-8) production compared to smoother surfaces.

3.3. Blood-implant interactions modulate the response of human gingival keratinocytes to Ti implant surfaces

This study highlights that while blood-implant interactions enhanced the attachment of HGF to rougher surfaces, they have the inverse effect on HGKs. When culturing HGKs on Ti implants, cell attachment was preferential on the smooth Machined surface in comparison to the rougher surfaces (SLA$_{Hphob}$, and SLActive$_{Hphil}$NS) (Fig. 4A), with the cells developing an elongated cobble-like morphology, aligned to the microscale surface features. On the rougher surfaces, HGKs showed a stochastic spreading pattern, limited attachment, and appeared smaller in size. This is in-line with previous work showing that nano-structured Ti surfaces poorly support the adherence of HGKs after 24 h of culture [47]. Previously, it has been suggested that keratinocyte adhesion to titanium surfaces relies on close cell-to-cell contact, extracellular matrix contacts, and by means of hemidesmosomes, all factors that would be impeded on rougher surfaces [48,49]. Blood pre-incubation negatively affected HGK attachment to all surfaces. Despite successfully attaching to all surfaces by 24 h (Fig. 4A), fewer nuclei were found on rougher surfaces by day 7, and the formation of an epithelial monolayer was only evident on the Machined surfaces (Fig. 4B). Similarly, only the Machined surface was found to be capable of supporting HGK proliferation, with a significant increase in the DNA mass of HGKs observed between day 1 and 7 (Fig. 4C). The SLA$_{Hphob}$ surface showed a constant DNA mass, while on the SLActive$_{Hphil}$NS surface a decrease in DNA mass between day 1 and 7 could be observed (Fig. 4C). These findings can be explained by a previous study showing that fibrinogen and fibrin are anti-adhesive for keratinocytes, and that during cutaneous wound repair, keratinocytes avoid the fibrin-rich clot as they do not express functional fibrinogen/fibrin receptors, specifically the αvβ3 integrin, and instead migrate over fibronectin-rich granulation tissue [50].
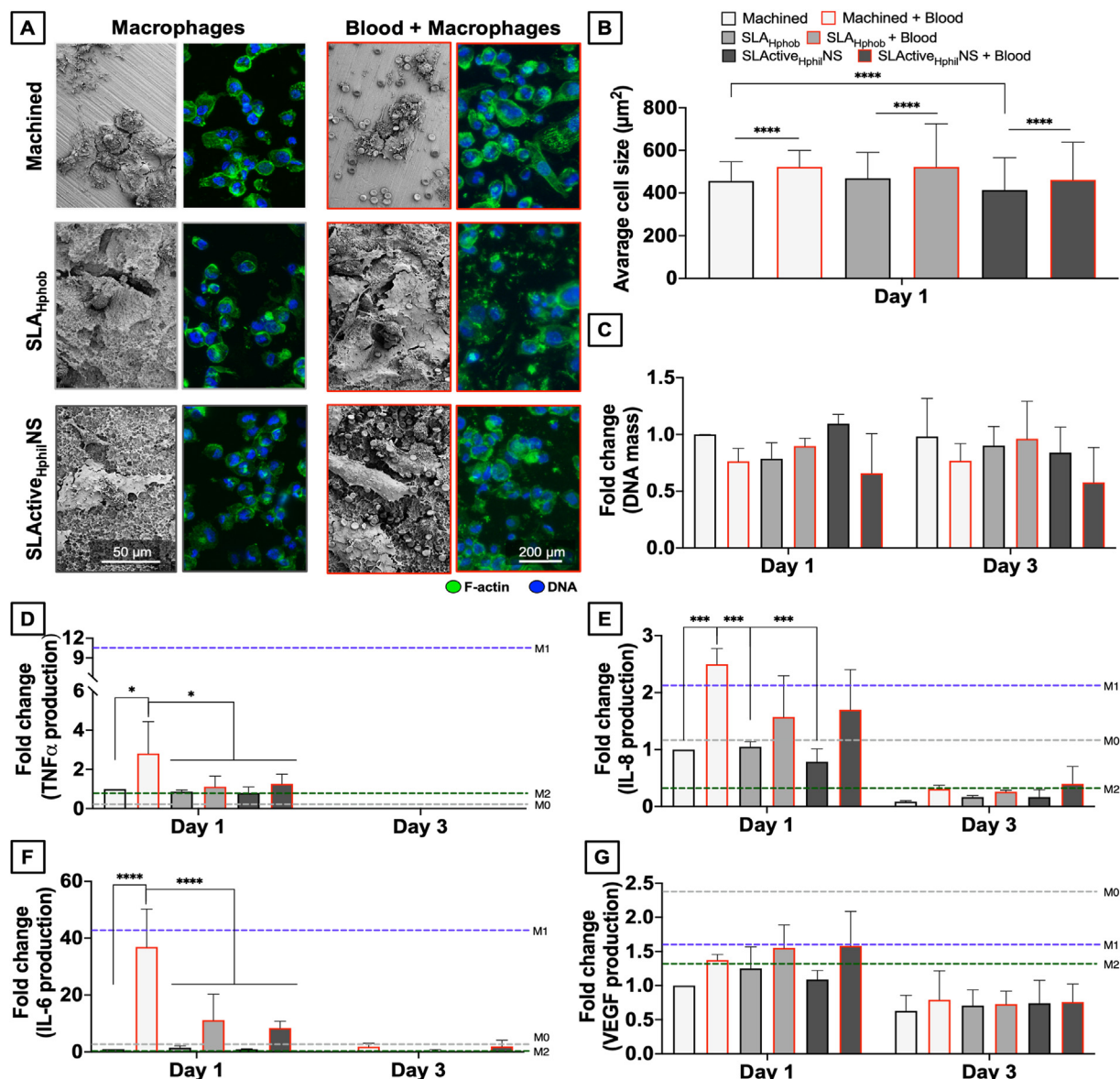

Fig. 5. The effect of blood-implant interactions on the attachment, proliferation, and cytokine production of macrophage-like cells in response to Ti implant surfaces. (A) SEM and CLSM images showing the morphology of macrophage-like cells, in the presence and absence of blood. Cells were stained for their cytoskeleton (green) and nuclei (blue). (B) Average cell size of cells attached to Ti implant surfaces, in the presence and absence of blood, after 24 h. Fold change of (C) DNA mass, (D) TNFα production, (E) IL-8 production, (F) IL-6 production, and (G) VEGF production after 1 and 3 days, normalized to cells on the Machined surface. The average level of TNFα, IL-8, IL-6, and VEGF produced by M0 (non-activated), M1-like and M2-like polarized cells on TCP are shown in each graph (dashed lines).

In the absence of blood, HGKs on the Machined surface showed a limited production of VEGF (20 pg/mL), IL-8 (83 pg/mL), and IL-6 (61 pg/mL), after 3 days (Fig. 4D-*F*). After 7 days, the levels of IL-8, IL-6, and VEGF, were significantly increased by 16.9-fold, 20.2-fold, and 9.3-fold (Fig. 4D–F), respectively, and were also significantly higher than the levels on the rougher surfaces. On Machined surfaces, the presence of blood did not affect the concentration of IL-8 and IL-6, but resulted in a significant decrease in the production of VEGF. On rougher surfaces, despite few HGKs remaining attached on the surface, the presence of blood enhanced the production of IL-8 by 4.5-fold on the SLA$_{Hphob}$ and 5.7-fold on the SLActive$_{Hphil}$NS, after 7 days. The stimulation of these factors indicate a pro-inflammatory response to the surface [51]. Taken together, HGKs represent a particularly sensitive cell type to Ti implant surface properties, and blood-implant interactions, whereby smoother surfaces with limited fibrin network present more favourable conditions for their attachment.

3.4. Blood-implant interactions modulate the response of human macrophage-like cells to Ti implant surfaces

Optimizing implant surface properties to steer the immune response to an implant has been an area of increasing research focus [52]. The innate immune response to an implant involves different cells, including neutrophils, dendritic cells, NK cells, and macrophages. Of these, macrophages have been shown to be key modulators of wound healing with their capacity to polarize towards pro- and anti-inflammatory phenotypes [36,53].

In the absence of blood, the attachment of macrophage-like cells was similar across all three surfaces with a round-shaped morphology and a limited number of lamellipodial and filopodial extensions (Fig. 5A). In the presence of blood, the macrophage-like cells had a similar morphology, but they were significantly larger in comparison to cells on Ti implant surfaces in the absence of blood (Fig. 5B). As expected after PMA-induced differentiation of THP-1 cells [54], the macrophage-like cells did not proliferate on any surface as indicated by their stagnant DNA levels between day 1 and 3 (Fig. 5C).

In the absence of blood, macrophage-like cells on the Machined surface showed a substantial production of TNFα (93 pg/mL), IL-8 (9770 pg/mL), IL-6 (12 pg/mL), and VEGF (306 pg/mL), after 24 h (Fig. 5D, E, *5F*, and *5G*). In comparison, rougher surfaces did not stimulate an increase nor decrease of these cytokines by more than 2-fold or less than 0.5-fold. While the presence of blood did not stimulate a significant change in the production of VEGF by macrophage-like cells on the Machined surface (Fig. 5G), the production of TNFα, IL-8, and IL-6 was significantly enhanced by 3.2-fold (Figs. 5D), 2.5-fold (Figs. 5E), and 36.9-fold (Fig. 5F), respectively. A previous study has shown varying levels of pro-inflammatory cytokines produced by rodent bone marrow-derived macrophages in response to SLA-Hphob, and SLActive-H$_{phil}$NS [55], while in this study such differences could not be reproduced in terms of IL-6, TNFα and IL-8 production. This discrepancy can be explained by the fact that in the previous report, investigators used M1-like and M2-like pre-polarized macrophages [55], whereas in this study M0 macrophage-like cells were seeded on the different surfaces. Nonetheless, the levels of TNFα and IL-6 produced by macrophage-like cells on the
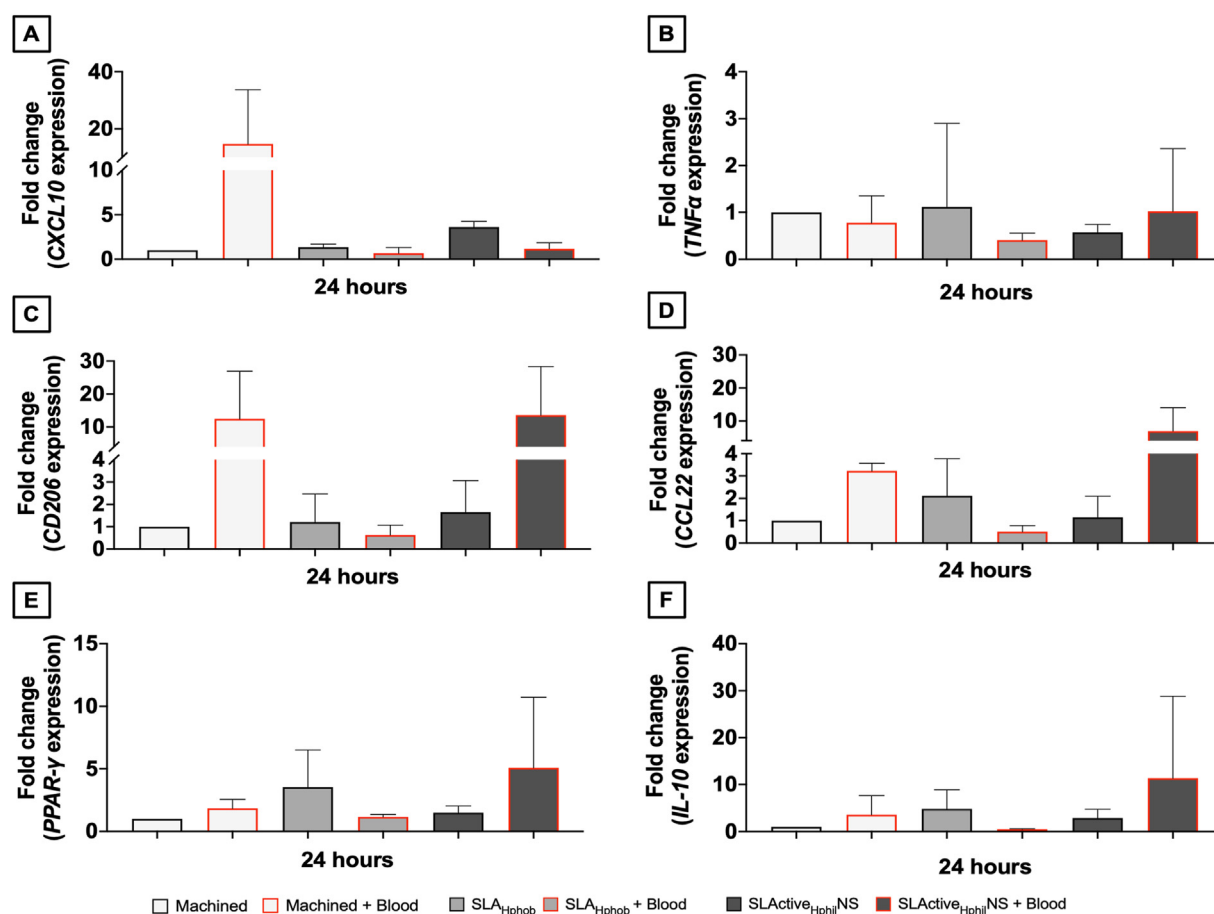

Fig. 6. The effect of blood-implant interactions on the gene expression of macrophage-like cells in response to Ti implant surfaces. Fold change of (A) *CXCL10*, (B) *TNFα*, (C) *CD206*, (D) *CCL22*, (E) *PPAR-γ*, and (F) *IL-10* gene expression after 24 h, normalized to macrophage-like cells on the Machined surface.

Machined surface pre-incubated with blood were significantly higher than the levels produced on the rougher surfaces in the same condition. This indicates that macrophage-like cell adhesion to a denser fibrin network reduces the production of pro-inflammatory cytokines, an observation that was also recently reported [56]. After 3 days, the production activity of all cytokines assessed had significantly decreased, in comparison to the level observed after 24 h, on all surfaces in all conditions. In particular, TNFα was no longer detectable by day 3, further suggesting a decrease of macrophage-like cell activity.

When assessing the expression of pro- and anti-inflammatory genes in macrophage-like cells cultured on the different implant surfaces in the absence of blood, pro-inflammatory gene *CXCL10* (Fig. 6A), and anti-inflammatory genes, *CD206* (Fig. 6C)*, CCL22* (Fig. 6D), *PPAR-γ* (Fig. 6E), and IL-10 (Fig. 6F), were found to be upregulated on rougher surfaces, SLA$_{Hphob}$, and SLActive$_{HphilNS}$, compared to the smoother Machined surface, but by less than a factor of 5 in each case. The expression of pro-inflammatory *TNF-α* was not regulated by any surface or condition. Previously, it has been shown that a narrow range of roughness ($R_a = 0.51–1.36\ \mu m$), which is comparable to that of the rough surfaces in this study, can polarize macrophages towards an anti-inflammatory M2-like state [23]. However, this study could not support this claim in the absence of blood.

In the presence of blood, the expression of the pro-inflammatory gene *CXCL10* was upregulated 14.7-fold on the Machined surface, while on rougher surfaces the presence of blood had a limited impact (Fig. 6A). Additionally, blood also led to the upregulated the expression of anti-inflammatory genes *CD206* (Fig. 6C)*, CCL22* (Fig. 6D), *PPAR-γ* (Fig. 6E), and IL-10 (Fig. 6F), which was especially evident on the hydrophilic SLActive$_{HphilNS}$ surface. Hydrophilic surfaces were previously shown to stimulate anti-inflammatory macrophage activation, more so on surfaces with microscale features compared to hydrophilic smooth surfaces [15]. However, the mentioned report did not take into account the blood response, and the fold changes in gene expression observed were generally much less than in this study. Taken together, this suggests that rough and hydrophilic surfaces stimulate macrophage-like cell polarization towards an M2-like phenotype, only in the presence of blood-implant interactions, while smoother surfaces, stimulate polarization towards an M1-like phenotype. The findings of this study come with the caveat of being derived from only a limited number of blood donors, yet they still indicate how implant surface properties could potentially steer inflammatory responses towards them.

This study was performed using 2-dimensional surfaces evaluating the response of single cell types, marking a contrast to the 3-dimensional interface that gingival tissue, and its multiple cell types, will form with an implant *in vivo*. In order to more closely understand the gingival healing process during implant integration, other studies have investigated how varying implant surface properties can influence tissue level response using 3D gingiva models [17]. However, such 3D models had limited sensitivity to changes in implant surface properties, suggesting that perhaps the influence of cell-to-cell interactions can be assessed using extensions of the models from this study in a co-culture, or even *trans-culture* format. Additional consideration should also be given to the apparent polar differences between soft and hard tissue's preferred implant surface properties, the variety of blood-implant interactions that can be expected on multi-level implants, and the cross-talk between cells adhering to different parts of such implants. Modern manufacturing techniques such as laser-texturing could enable the production of surface property gradients to facilitate optimal implant integration with both soft tissue and the underlying bone.

4. Conclusion

This study demonstrates that while implant surface properties can steer the biological response of soft tissue cells, including gingival fibroblasts, keratinocytes and macrophage-like cells, this response can be significantly modulated by blood-implant interactions, generating a more physiologically relevant *in vitro* platform for the evaluation of an implant's soft tissue integration potential. This study highlights the importance blood-implant interactions, which are heavily dependent on an implant's surface properties, and proposes that they should be taken into account in future implant developments.

Authorship contribution statement

William A. Lackington: Conceptualization, methodology, investigation, data curation, formal analysis, writing, review and editing. Lada Fleyshman: Data curation, methodology, investigation, writing. Peter Schweizer: Methodology, investigation, resources, data curation. Yvonne Elbs-Glatz: Investigation, methodology, resources. Stefanie Guimond: Investigation, methodology, resources. Markus Rottmar: Conceptualization, funding acquisition, resources, data curation, supervision, writing, review and editing.

Declaration of competing interest

The authors declare that they have no known competing financial interests or personal relationships that could have appeared to influence the work reported in this paper.

Acknowledgements

References

[1] C.E. Misch, Dental Implant Prosthetics, second ed., Elsevier, St.Louis, Missouri, 2015.

[2] S. Goktas, J.J. Dmytryk, P.S. McFetridge, Biomechanical behavior of oral soft tissues, J. Periodontol. 82 (2011) 1178–1186, https://doi.org/10.1902/jop.2011.100573.

[3] X. Gao, M. Fraulob, G. Haïat, Biomechanical behaviours of the bone-implant interface: a review, J. R. Soc. Interface 16 (2019), https://doi.org/10.1098/rsif.2019.0259.

[4] J.W. Nicholson, Titanium alloys for dental implants: a review, Prosthesis 2 (2020) 100–116, https://doi.org/10.3390/prosthesis2020011.

[5] J.S. Colombo, S. Satoshi, J. Okazaki, S.J. Crean, A.J. Sloan, R.J. Waddington, In vivo monitoring of the bone healing process around different titanium alloy implant surfaces placed into fresh extraction sockets, J. Dent. 40 (2012) 338–346, https://doi.org/10.1016/j.jdent.2012.01.010.

[6] D.D. Bosshardt, V. Chappuis, D. Buser, Osseointegration of titanium, titanium alloy and zirconia dental implants: current knowledge and open questions, Periodontol 73 (2000) 22–40, https://doi.org/10.1111/prd.12179, 2017.

[7] P. Nicolau, F. Guerra, R. Reis, T. Krafft, K. Benz, J. Jackowski, 10-year outcomes with immediate and early loaded implants with a chemically modified SLA surface, Quintessence Int. 50 (2019) 114–124, https://doi.org/10.3290/j.qi.a41664.

[8] B.S. Talwar, A focus on soft tissue in dental implantology, J. Indian Prosthodont. Soc. 12 (2012) 137–142, https://doi.org/10.1007/s13191-012-0133-x.

[9] M. Rakic, P. Galindo-Moreno, A. Monje, S. Radovanovic, H.L. Wang, D. Cochran, A. Sculean, L. Canullo, How frequent does peri-implantitis occur? A systematic review and meta-analysis, Clin. Oral Invest. 22 (2018) 1805–1816, https://doi.org/10.1007/s00784-017-2276-y.

[10] S.L. Oh, H.J. Shiau, M.A. Reynolds, Survival of dental implants at sites after implant failure: a systematic review, J. Prosthet. Dent 123 (2020) 54–60, https://doi.org/10.1016/j.prosdent.2018.11.007.

[11] B.S. Kopf, A. Schipanski, M. Rottmar, S. Berner, K. Maniura-Weber, Enhanced differentiation of human osteoblasts on Ti surfaces pre-treated with human whole blood, Acta Biomater. 19 (2015) 180–190, https://doi.org/10.1016/j.actbio.2015.03.022.

[12] A.B. Faia-Torres, S. Guimond-Lischer, M. Rottmar, M. Charnley, T. Goren, K. Maniura-Weber, N.D. Spencer, R.L. Reis, M. Textor, N.M. Neves, Differential regulation of osteogenic differentiation of stem cells on surface roughness gradients, Biomaterials 35 (2014) 9023–9032, https://doi.org/10.1016/j.biomaterials.2014.07.015.

[13] V. Milleret, P.S. Lienemann, A. Gasser, S. Bauer, M. Ehrbar, A. Wennerberg, Rational design and in vitro characterization of novel dental implant and abutment surfaces for balancing clinical and biological needs, Clin. Implant Dent. Relat. Res. 21 (Suppl 1) (2019) 15–24, https://doi.org/10.1111/cid.12736.

[14] J.I. Rosales-Leal, M.A. Rodríguez-Valverde, G. Mazzaglia, P.J. Ramón-Torregrosa, L. Díaz-Rodríguez, O. García-Martínez, M. Vallecillo-Capilla, C. Ruiz,

M.A. Cabrerizo-Vílchez, Effect of roughness, wettability and morphology of engineered titanium surfaces on osteoblast-like cell adhesion, Colloids Surfaces A Physicochem. Eng. Asp. 365 (2010) 222–229, https://doi.org/10.1016/j.colsurfa.2009.12.017.

[15] K.M. Hotchkiss, G.B. Reddy, S.L. Hyzy, Z. Schwartz, B.D. Boyan, R. Olivares-Navarrete, A.B. Author, Titanium surface characteristics, including topography and wettability, alter macrophage activation graphical abstract HHS public access author manuscript, Acta Biomater. 31 (2016) 425–434, https://doi.org/10.1016/j.actbio.2015.12.003.Titanium.

[16] A. Wennerberg, R. Jimbo, S. Stübinger, M. Obrecht, M. Dard, S. Berner, Nanostructures and hydrophilicity influence osseointegration: a biomechanical study in the rabbit tibia, Clin. Oral Implants Res. 25 (2014) 1041–1050, https://doi.org/10.1111/clr.12213.

[17] J.K. Buskermolen, C.M.A. Reijnders, S.W. Spiekstra, T. Steinberg, C.J. Kleverlaan, A.J. Feilzer, A.D. Bakker, S. Gibbs, Development of a full-thickness human gingiva equivalent constructed from immortalized keratinocytes and fibroblasts, Tissue Eng. C Methods 22 (2016) 781–791, https://doi.org/10.1089/ten.TEC.2016.0066.

[18] B. Zhao, H.C. Van Der Mei, G. Subbiahdoss, J. De Vries, M. Rustema-Abbing, R. Kuijer, H.J. Busscher, Y. Ren, Soft tissue integration versus early biofilm formation on different dental implant materials, Dent. Mater. 30 (2014) 716–727, https://doi.org/10.1016/j.dental.2014.04.001.

[19] M. Köunönen, M. Hormia, J. Kivilahti, J. Hautaniemi, I. Thesleff, Effect of surface processing on the attachment, orientation, and proliferation of human gingival fibroblasts on titanium, J. Biomed. Mater. Res. 26 (1992) 1325–1341, https://doi.org/10.1002/jbm.820261006.

[20] G. Lauer, M. Wiedmann-Al-Ahmad, J.E. Otten, U. Hübner, R. Schmelzeisen, W. Schilli, The titanium surface texture effects adherence and growth of human gingival keratinocytes and human maxillar osteoblast-like cells in vitro, Biomaterials 22 (2001) 2799–2809, https://doi.org/10.1016/S0142-9612(01)00024-2.

[21] S. Ferraris, F. Warchomicka, C. Ramskogler, M. Tortello, A. Cochis, A. Scalia, G. Gautier di Confiengo, J. Keckes, L. Rimondini, S. Spriano, Surface structuring by Electron Beam for improved soft tissues adhesion and reduced bacterial contamination on Ti-grade 2, J. Mater. Process. Technol. 266 (2019) 518–529, https://doi.org/10.1016/j.jmatprotec.2018.11.026.

[22] S. Ferraris, V. Guarino, A. Cochis, A. Varesano, I. Cruz Maya, C. Vineis, L. Rimondini, S. Spriano, Aligned keratin submicrometric-fibers for fibroblasts guidance onto nanogrooved titanium surfaces for transmucosal implants, Mater. Lett. 229 (2018) 1–4, https://doi.org/10.1016/j.matlet.2018.06.103.

[23] Y. Zhang, X. Cheng, J.A. Jansen, F. Yang, J.J.J.P. van den Beucken, Titanium surfaces characteristics modulate macrophage polarization, Mater. Sci. Eng. C 95 (2019) 143–151, https://doi.org/10.1016/j.msec.2018.10.065.

[24] M. Rottmar, E. Müller, S. Guimond-Lischer, M. Stephan, S. Berner, K. Maniura-Weber, Assessing the osteogenic potential of zirconia and titanium surfaces with an advanced in vitro model, Dent. Mater. 35 (2019) 74–86, https://doi.org/10.1016/j.dental.2018.10.008.

[25] M.A. Burkhardt, J. Waser, V. Milleret, I. Gerber, M.Y. Emmert, J. Foolen, S.P. Hoerstrup, F. Schlottig, V. Vogel, Synergistic interactions of blood-borne immune cells, fibroblasts and extracellular matrix drive repair in an in vitro peri-implant wound healing model, Sci. Rep. 6 (2016) 1–15, https://doi.org/10.1038/srep21071.

[26] V. Malheiro, Y. Elbs-Glatz, M. Obarzanek-Fojt, K. Maniura-Weber, A. Bruinink, Harvesting pre-polarized macrophages using thermo-responsive substrates, Sci. Rep. 7 (2017) 42495, https://doi.org/10.1038/srep42495.

[27] Y. Gu, J. Du, M. Si, J. Mo, S. Qiao, H. Lai, The roles of PI3K/Akt signaling pathway in regulating MC3T3-E1 preosteoblast proliferation and differentiation on SLA and SLActive titanium surfaces, J. Biomed. Mater. Res. 101 (2013) 748–754.

[28] I.D. Sener-Yamaner, G. Yamaner, A. Sertgöz, C.F. Çanakçi, M. Özcan, Marginal bone loss around early-loaded SLA and SLActive implants: radiological follow-up evaluation up to 6.5 years, Implant Dent. 26 (2017) 592–599.

[29] C.A. Schneider, W.S. Rasband, K.W. Eliceiri, NIH Image to ImageJ: 25 years of image analysis, Nat. Methods 9 (2012) 671–675, https://doi.org/10.1038/nmeth.2089.

[30] M.A. Burkhardt, I. Gerber, C. Moshfegh, M.S. Lucas, J. Waser, M.Y. Emmert, S.P. Hoerstrup, F. Schlottig, V. Vogel, Clot-entrapped blood cells in synergy with human mesenchymal stem cells create a pro-angiogenic healing response, Biomater. Sci. 5 (2017) 2009–2023, https://doi.org/10.1039/c7bm00276a.

[31] M.S. Lord, M. Foss, F. Besenbacher, Influence of nanoscale surface topography on protein adsorption and cellular response, Nano Today 5 (2010) 66–78, https://doi.org/10.1016/j.nantod.2010.01.001.

[32] T.A. Horbett, Fibrinogen adsorption to biomaterials, J. Biomed. Mater. Res. A. 106 (2018) 2777–2788, https://doi.org/10.1002/jbm.a.36460.

[33] D. Di Iorio, T. Traini, M. Degidi, S. Caputi, J. Neugebauer, A. Piattelli, Quantitative evaluation of the fibrin clot extension on different implant surfaces: an in vitro study, J. Biomed. Mater. Res. B Appl. Biomater. 74 (2005) 636–642, https://doi.org/10.1002/jbm.b.30251.

[34] R. Sridharan, A.R. Cameron, D.J. Kelly, C.J. Kearney, F.J. O'Brien, Biomaterial based modulation of macrophage polarization: a review and suggested design principles, Mater. Today 18 (2015) 313–325, https://doi.org/10.1016/j.mattod.2015.01.019.

[35] R. Olivares-Navarrete, S.L. Hyzy, P.J. Slosar, J.M. Schneider, Z. Schwartz, B.D. Boyan, Implant materials generate different peri-implant inflammatory factors: poly-ether-ether-ketone promotes fibrosis and microtextured titanium promotes osteogenic factors, Spine (Phila. Pa. 1976 40 (2015) 399.

[36] F. Billing, M. Jakobi, D. Martin, K. Gerlach, E. Arefaine, M. Weiss, N. Schneiderhan-Marra, H. Hartmann, C. Shipp, The immune response to the SLActive titanium dental implant surface in vitro is predominantly driven by innate immune cells, J. Immunol. Regen. Med. 13 (2021) 100047, https://doi.org/10.1016/j.regen.2021.100047.

[37] H.N. Nguyen, E.H. Noss, F. Mizoguchi, C. Huppertz, K.S. Wei, G.F.M. Watts, M.B. Brenner, Autocrine loop involving IL-6 family member LIF, LIF receptor, and STAT4 drives sustained fibroblast production of inflammatory mediators, Immunity 46 (2017) 220–232, https://doi.org/10.1016/j.immuni.2017.01.004.

[38] D.R.J. Verboogen, N.H. Revelo, M. Ter Beest, G. Van Den Bogaart, Interleukin-6 secretion is limited by self-signaling in endosomes, J. Mol. Cell Biol. 11 (2018) 144–157, https://doi.org/10.1093/jmcb/mjy038.

[39] S. Ferraris, F. Truffa Giachet, M. Miola, E. Bertone, A. Varesano, C. Vineis, A. Cochis, R. Sorrentino, L. Rimondini, S. Spriano, Nanogrooves and keratin nanofibers on titanium surfaces aimed at driving gingival fibroblasts alignment and proliferation without increasing bacterial adhesion, Mater. Sci. Eng. C 76 (2017) 1–12, https://doi.org/10.1016/j.msec.2017.02.152.

[40] S. Ferraris, A. Cochis, M. Cazzola, M. Tortello, A. Scalia, S. Spriano, L. Rimondini, Cytocompatible and anti-bacterial adhesion nanotextured titanium oxide layer on titanium surfaces for dental and orthopedic implants, Front. Bioeng. Biotechnol. 7 (2019), https://doi.org/10.3389/fbioe.2019.00103.

[41] A.C. De Luca, M. Zink, A. Weidt, S.G. Mayr, A.E. Markaki, Effect of microgrooved surface topography on osteoblast maturation and protein adsorption, J. Biomed. Mater. Res. 103 (2015) 2689–2700.

[42] C.J. Oates, W. Wen, D.W. Hamilton, Role of titanium surface topography and surface wettability on focal adhesion kinase mediated signaling in fibroblasts, Mater. (Basel, Switzerland) 4 (2011) 893–907, https://doi.org/10.3390/ma4050893.

[43] I. Narimatsu, I. Atsuta, Y. Ayukawa, W. Oshiro, N. Yasunami, A. Furuhashi, K. Koyano, Epithelial and connective tissue sealing around titanium implants with various typical surface finishes, ACS Biomater. Sci. Eng. 5 (2019) 4976–4984, https://doi.org/10.1021/acsbiomaterials.9b00499.

[44] J. Wei, T. Igarashi, N. Okumori, T. Igarashi, T. Maetani, B. Liu, M. Yoshinari, Influence of surface wettability on competitive protein adsorption and initial attachment of osteoblasts, Biomed. Mater. 4 (2009), https://doi.org/10.1088/1748-6041/4/4/045002, 0–7.

[45] W.S. To, K.S. Midwood, Plasma and cellular fibronectin: distinct and independent functions during tissue repair, Fibrogenesis Tissue Repair 4 (2011) 21, https://doi.org/10.1186/1755-1536-4-21.

[46] O. Andrukhov, C. Behm, A. Blufstein, C. Wehner, J. Gahn, B. Pippenger, R. Wagner, X. Rausch-Fan, Effect of implant surface material and roughness to the susceptibility of primary gingival fibroblasts to inflammatory stimuli, Dent. Mater. 36 (2020) e194–e205, https://doi.org/10.1016/j.dental.2020.04.003.

[47] M. Dorkhan, T. Yücel-Lindberg, J. Hall, G. Svensäter, J.R. Davies, Adherence of human oral keratinocytes and gingival fibroblasts to nano-structured titanium surfaces, BMC Oral Health 14 (2014) 1–9, https://doi.org/10.1186/1472-6831-14-75.

[48] M. Hormia, M. Könönen, J. Kivilahti, I. Virtanen, Immunolocalization of proteins specific for adhaerens junctions in human gingival epithelial cells grown on differently processed titanium surfaces, J. Periodontal. Res. 26 (1991) 491–497, https://doi.org/10.1111/j.1600-0765.1991.tb01800.x.

[49] J.T. Elder, S. Kansra, S.W. Stoll, Autocrine regulation of keratinocyte proliferation, J. Clin. Ligand Assay 27 (2004) 137–142.

[50] M. Kubo, L. Van De Water, L.C. Plantefaber, M.W. Mosesson, M. Simon, M.G. Tonnesen, L. Taichman, R.A.F. Clark, Fibrinogen and fibrin are anti-adhesive for keratinocytes: a mechanism for fibrin eschar slough during wound repair, J. Invest. Dermatol. 117 (2001) 1369–1381, https://doi.org/10.1046/j.0022-202x.2001.01551.

[51] J. Steude, R. Kulke, E. Christophers, Interleukin-1-stimulated secretion of interleukin-8 and growth-related oncogene-α demonstrates greatly enhanced keratinocyte growth in human raft cultured epidermis, J. Invest. Dermatol. 119 (2002) 1254–1260, https://doi.org/10.1046/j.1523-1747.2002.19616.

[52] M. Rahmati, M.J. Frank, S.M. Walter, M.C. Monjo, M. Satué, J.E. Reseland, S.P. Lyngstadaas, H.J. Haugen, Osteoimmunomodulatory effects of enamel matrix derivate and strontium coating layers: a short- and long-term in vivo study, ACS Appl. Bio Mater. 3 (2020) 5169–5181, https://doi.org/10.1021/acsabm.0c00608.

[53] G.J. Kotwal, S. Chien, Macrophage differentiation in normal and accelerated wound healing, results probl, Cell Differ. 62 (2017) 353–364, https://doi.org/10.1007/978-3-319-54090-0_14.

[54] E. Richter, K. Ventz, M. Harms, J. Mostertz, F. Hochgräfe, Induction of macrophage function in human THP-1 cells is associated with rewiring of MAPK signaling and activation of MAP3K7 (TAK1) protein kinase, Front. Cell Dev. Biol. 4 (2016). https://www.frontiersin.org/article/10.3389/fcell.2016.00021.

[55] S.M. Hamlet, R.S.B. Lee, H.-J. Moon, M.A. Alfarsi, S. Ivanovski, Hydrophilic titanium surface-induced macrophage modulation promotes pro-osteogenic signalling, Clin. Oral Implants Res. 30 (2019) 1085–1096, https://doi.org/10.1111/clr.13522.

[56] J.Y. Hsieh, T.D. Smith, V.S. Meli, T.N. Tran, E.L. Botvinick, W.F. Liu, Differential regulation of macrophage inflammatory activation by fibrin and fibrinogen, Acta Biomater. 47 (2017) 14–24, https://doi.org/10.1016/j.actbio.2016.09.024.